Brain Struct Funct
DOI 10.1007/s00429-014-0971-x

ORIGINAL ARTICLE

Structural and functional connectivity mapping of the vestibular circuitry from human brainstem to cortex

V. Kirsch · D. Keeser · T. Hergenroeder · O. Erat · B. Ertl-Wagner · T. Brandt · M. Dieterich

Received: 19 May 2014 / Accepted: 17 December 2014

Abstract Structural and functional interconnections of the bilateral central vestibular network have not yet been completely delineated. This includes both ipsilateral and contralateral pathways and crossing sites on the way from the vestibular nuclei via the thalamic relay stations to multiple "vestibular cortex" areas. This study investigated "vestibular" connectivity in the living human brain in between the vestibular nuclei and the parieto-insular vestibular cortex (PIVC) by combined structural and functional connectivity mapping using diffusion tensor imaging and functional connectivity magnetic resonance imaging in 24 healthy right-handed volunteers. We observed a congruent functional and structural link between the vestibular nuclei and the ipsilateral and contralateral PIVC. Five separate and distinct vestibular pathways were identified: three run ipsilaterally, while the two others cross either in the pons or the midbrain. Two of the ipsilateral projections run through the posterolateral or paramedian thalamic subnuclei, while the third bypasses the thalamus to reach the inferior part of the insular cortex directly. Both contralateral pathways travel through the posterolateral thalamus. At the cortical level, the PIVC regions of both hemispheres with a right hemispherical dominance are interconnected transcallosally through the antero-caudal splenium. The above-described bilateral vestibular circuitry in its entirety takes the form of a structure of a rope ladder extending from the brainstem to the cortex with three crossings in the brainstem (vestibular nuclei, pons, midbrain), none at thalamic level and a fourth cortical crossing through the splenium of the corpus callosum.

Keywords Vestibular system · Vestibular pathways · Vestibular thalamus · Vestibular cortex · Structural and functional connectivity mapping

Abbreviations

III	Oculomotor nucleus
VII	Facial nucleus
NVIII	Vestibular nerve
BA	Brodmann area
BIC	Brachium of the inferior colliculus
CCN	Central caudal nucleus
CCT	Cerebellothalamic tractotomy
CL	Central lateral nucleus (posterior part)
CLi	Caudal linear nucleus

V. Kirsch (✉) · T. Hergenroeder · O. Erat · M. Dieterich
Department of Neurology, University Hospital, Ludwig-Maximilians University, Marchioninistraße 15, 81377 Munich, Germany
e-mail: valerie.kirsch@med.lmu.de

V. Kirsch · M. Dieterich
Graduate School of Systemic Neuroscience, Ludwig-Maximilians University, Munich, Germany

V. Kirsch · B. Ertl-Wagner · T. Brandt · M. Dieterich
German Center for Vertigo and Balance Disorders-IFBLMU, Ludwig-Maximilians University, Munich, Germany

D. Keeser · B. Ertl-Wagner
Department of Radiology, Ludwig-Maximilians University, Munich, Germany

D. Keeser
Department of Psychiatry, Ludwig-Maximilians University, Munich, Germany

T. Brandt
Clinical Neuroscience, Ludwig-Maximilians University, 81377 Munich, Germany

M. Dieterich
Munich Cluster for Systems Neurology (SyNergy), Munich, Germany

Published online: 01 January 2015

CM	Centre médian nucleus (or centromedian)
CP	Cerebral peduncle
DRd	Dorsal raphe nucleus, dorsal part
DTI	Diffusion tensor imaging
fcMRI	Functional connectivity magnetic resonance imaging
Gi	Gigantocellular nucleus
IC	Internal capsule
INC	Interstitial nucleus of Cajal
L	Left
LP	Lateral posterior nucleus
LSO	Lateral superior olivary nucleus
LVN	Lateral vestibular nerve
MesV	Mesencephalic trigeminal nucleus
ML	Medial lemniscus
MLF	Medial longitudinal fascicle
MRF	Mesencephalic longitudinal formation
MRFv	Mesencephalic longitudinal formation, ventral part
MSO	Medial superior olivary nucleus
MVN	Medial vestibular nerve
nBIC	Nucleus of the brachium of the inferior colliculus
OTR	Ocular tilt reaction
PAGl	Periaqueductal gray, lateral part
PAGm	Periaqueductal gray, medial part
PCR	Parvocellular reticular nucleus
PET	Positron emission tomography
PGiD	Dorsal paragigantocellular nucleus
PIVC	Parieto-insular vestibular cortex
PN	Pontine nuclei
Po	Posterior nucleus
POC	Periolivary complex
PPTd	Pedunculopontine nucleus, pars dissipata
PrP	Prepositus nucleus
PuA	Anterior pulvinar
PuL	Lateral pulvinar
PuM	Medial pulvinar
R	Right
riMLF	Rostral interstitial nucleus of medial longitudinal fasciculus
ROI	Region of interest
RSN	Resting-state networks
Rt	Reticular thalamic nucleus
Ru	Nucleus ruber tegmenti
SC	Superior colliculus
SCP	Superior cerebellar peduncle
SEL	Subependymal layer
SNc	Substantia nigra, pars compacta (ventral tier pars α and dorsal tier pars β)
SpVo	Spinal trigeminal nucleus, oral part
SVV	Subjective visual vertical
TSpV	Spinal trigeminal tract
VBLM	Voxel-based lesion mapping
Vim	Ventrointermedial nucleus, part of VPL
VL	Ventral lateral nucleus
VN-L	Left vestibular nucleus
VN-R	Right vestibular nucleus
VOG	Videooculography
VOR	Vestibular–ocular reflex
VPLp	Ventral posterior lateral nucleus (posterior and anterior divisions)
VPLv	Ventral posterior lateral nucleus (posterior and anterior divisions)
VPM	Ventral posterior medial nucleus
Zi	Zona incerta

Introduction

To maintain orientation and balance, the human brain integrates vestibular, visual, and somatosensory information in a multilevel sensorimotor network (Guldin et al. 1992; Eggers and Zee 2010). The vestibular system provides the brain with sensory signals about three-dimensional head rotations and translations to adjust the eyes, head, and body to the upright position within the gravitational field. Further vestibular input is essential to mediate higher cognitive functions such as the perception of verticality (Baier et al. 2012), self-motion (Chen et al. 2011a), spatial memory, orientation, and navigation (Dieterich and Brandt 1993a; Green and Angelaki 2004). Compared to descriptions of other sensory systems, many details of the exact location and subfunction of vestibular structures in humans are still lacking, especially their ipsilateral and contralateral interconnections (Dieterich and Brandt 2008; Lopez and Blanke 2011; zu Eulenburg et al. 2012).

Most of our current understanding of the human vestibular system has been derived from lesion, tracer, and electrophysiological studies in animals (Grüsser et al. 1990a, b; Büttner-Ennever 1992, 1999; Goldberg et al. 2012). Human homologs of parts of the known bilateral network in animals have been identified in the temporo-parietal cortex, especially around a core region in the posterior insula, the parieto-insular vestibular cortex (PIVC), in ischemic lesion studies (Brandt and Dieterich 1994; Dieterich and Brandt 2008) and paradigm-based PET and fMRI studies (Fasold et al. 2002; Emri et al. 2003; Dieterich 2007; zu Eulenburg et al. 2012). These regions of a comparable bilateral network of multiple multisensory vestibular cortex areas are connected ipsilaterally and contralaterally with the vestibular nuclei in the brainstem (Brandt and Dieterich 1994; Dieterich and Brandt 1993a; Zwergal et al. 2009; Baier et al. 2012).

The thalamus is an important structure within the vestibular network, because it serves as a relay station (Lang et al. 1979; Blum et al. 1979a) and as a "gatekeeper" for vestibular information (Dieterich et al. 2005). However, here too details of the involved vestibular thalamic subnuclei as well as the route of vestibular projections from the brainstem to the cortex (e.g., PIVC) and the existence of a potential projection bypassing the thalamus have not yet been defined (Dieterich et al. 2005; Lopez and Blanke 2011).

Therefore, combined structural and functional connectivity mapping (Greicius et al. 2009; van den Heuvel et al. 2009; Zhang et al. 2010) with diffusion tensor imaging (DTI) and functional connectivity magnetic resonance imaging (fcMRI) provides a tool (Behrens and Sporns 2012) for elucidating ipsi- and contralateral pathways and functional interrelations extending from the vestibular nuclei to the vestibular cortex areas in the living healthy brain. Hence in the context, we use the term "vestibular connectivity" in the understanding that this includes areas with multisensory convergences as a characteristic feature of the vestibular system (Chen et al. 2011b).

The main questions posed were as follows:

(i) Is there congruence between the functional and structural vestibular connectivity?
(ii) Do the fibers originating in the vestibular nuclei link to the core region of the PIVC?
(iii) How many fiber bundles can be topographically separated?
(iv) Which regions and nuclei of the brainstem and thalamus are involved?
(v) Are there multiple midline crossings of vestibular pathways and, if so, where are they located?
(vi) Is there an interhemispheric connection between the vestibular cortex regions, especially of the PIVCs?

Materials and methods

Subjects

Twenty-four healthy volunteers (11 females; aged 20–47 years, mean age 28.2 ± 6.3 years) were included in the study. Inclusion criteria were age between 18 and 50 years and right-handedness because of the earlier described right hemispheric vestibular dominance in right-handers and left hemispheric dominance in left-handers (Dieterich et al. 2003). The laterality quotient for right-handedness was assessed with the 10-item inventory of the Edinburgh test (Oldfield 1971; Salmaso and Longoni 1985). Exclusion criteria were a history of any neurological, vestibular, and/or psychiatric disorders and MR-related contraindications such as cardiac pacemakers, ferromagnetic implants, or claustrophobia. Institutional review board (IRB) approval was obtained prior to the initiation of the study. Each participant provided informed oral and written consent in accordance with the Declaration of Helsinki.

Measurement of the semicircular canal and otolith functions

The integrity of vestibular function was ascertained by assessing the semicircular canal function with the vestibulo-ocular reflex (VOR) and otolith function with the determination of the subjective visual vertical (SVV), respectively. The VOR was measured by the head- impulse test (Halmagyi and Curthoys 1988) using high-frame-rate video-oculography (VOG) with EyeSeeCam (Schneider et al. 2009; EyeSeeTech, Munich, Germany). A median gain during head impulses <0.8 (eye velocity in °/s divided by head velocity in °/s) was considered as the criterion for a pathological VOR and exclusion of the subject. A tilt of the SVV is a sensitive sign of a graviceptive vestibular tone imbalance, assessed when sitting in an upright position in front of a half-spherical dome with the head fixed on a chin rest (for details see: Dieterich and Brandt 1993a). A mean deviation of >2.5° from the true vertical was considered a pathological tilt of SVV.

MRI data acquisition

The combination of structural and functional connectivity mapping (Greicius et al. 2009; van den Heuvel et al. 2009; Zhang et al. 2010) with diffusion tensor imaging (DTI) and functional connectivity magnetic resonance imaging (fcMRI) provides information on functional and structural linkages between different areas of the brain. MR imaging data were acquired in a whole-body 3.0 Tesla MR scanner (Magnetom Verio, Siemens Healthcare, Erlangen, Germany) with a 32-channel head coil. Structural fiber tracts were assessed using a DTI sequence. Diffusivity was measured in 32 directions with 2.0 × 2.0 × 2.0 mm^3 isotropic voxels (TE = 110 ms, TR = 8,900 ms, b values = 0 and 1,000 s/mm^2). Intrinsic brain activity was assessed with BOLD fMRI based on a T2*-weighted echo-planar imaging (EPI) sequence with 3.0 × 3.0 × 3.0 mm^3 isotropic voxels (TE = 30 ms, TR = 3,000 ms, 200 frames per subject). No other task was required except keeping the eyes closed, remaining still, and not falling asleep. Anatomical images acquired for definitive atlas transformation included a T1-weighted magnetization-prepared rapid gradient echo (MP-RAGE) sequence with a field of view of 256 mm and an isotropic spatial resolution

of $1.0 \times 1.0 \times 1.0$ mm^3 (TE 4.37 ms, TR = 2,100 ms, number of slices 160). Images in DICOM format were converted to the NIfTI-file format.

Regions of interest (ROIs)

The major focus of our study was to delineate the structural and functional interconnections of the bilateral ipsilateral and contralateral pathways and the crossing sites in the brainstem on the way from the vestibular nuclei via its thalamic and extra-thalamic roots to the core of the "vestibular cortex" area network, which is thought to be the ipsilateral and contralateral parieto-insular vestibular cortex (PIVC). To ensure most possible congruence of the structural (DTI) and functional (fcMRI) connectivity maps, we chose a similar approach for both data sets. Functionally, we looked for linked synchronicity of neuronal activity between the vestibular nuclei and the rest of the brain, assuming that the PIVC would most probably be included in the results. Structurally, we set the vestibular nuclei as the seed and the PIVC as the target point. Brainstem and thalamus were set as waypoints, but were purposely chosen to be large and unspecific without implying presumptions of the possible vestibular fibers ensuring a near "data-driven" approach.

Vestibular nuclei seed ROIs (cp. Fig. 1e) were created in Mango (Multi-Image Analysis GUI) version 3.0.4 (ric.uthscsa.edu/mango) using a cubic diameter of 10 mm based on MNI coordinates ($x = -16/16$, $y = -36$, $z = -32$) published previously in Miller et al. 2008. The remaining ROIs were extracted from probabilistic atlases included within FSL (FMRIB Software Library) version 5.0 (Smith et al. 2004; Woolrich et al. 2009; Jenkinson et al. 2012), binarized to 10 (Hammers et al. 2003) and registered to the FSL Montreal Neurological Institute's (MNI) 152 subject templates. Subcortical ROIs, such as the brainstem and thalamus (cp. Fig. 1a, b), were extracted from the Harvard–Oxford subcortical structural atlas (Desikan et al. 2006; Makris et al. 2006). For the cortical core region of the PIVC, an ROI combined out of Ig1 (as posterior ventral insula) and operculum 2 (as adjacent retroinsular parietal operculum; cp. Fig. 1c) from the Juelich histological (cyto- and myelo-architectonic) atlas was used (Eickhoff et al. 2005, 2006a, b). However, DTI tractography is limited when tracking crossing and bending pathways (Johansen-Berg and Rushworth 2009). Therefore,

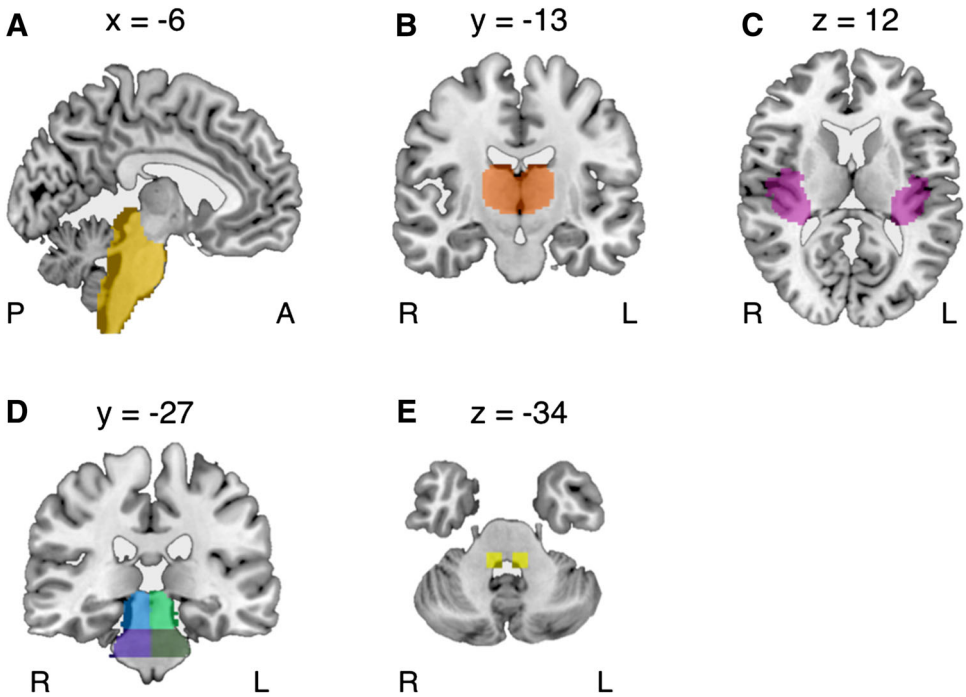

Fig. 1 DTI and fcMRI regions of interest (ROIs). Our approach to structural (**a**–**d**) and functional (**e**) regions of interest (ROIs) differed. Structurally, we aimed to tract the vestibular brainstem pathways projecting to the core region of the PIVC. Therefore, DTI ROIs were cerebral areas known to be involved in vestibular processing, such as the brainstem (**a**), thalamus (**b**), and parieto-insular vestibular cortex (PIVC, **c**). **d** The sectioned brainstem ROIs for the second more detailed DTI analysis concentrating on the crossing brainstem pathways. Functionally, we were interested in the synchronicity of neuronal activity between the vestibular nuclei and distinct cortical or subcortical brain regions during a period of rest. Hence, the vestibular nuclei fcMRI seed ROIs (**e**) were cubic diameter of 10 mm around coordinates of the vestibular nuclei ($x = -16/16$, $y = -36$, $z = -32$) published prior (Miller et al. 2008)

further DTI analyses focusing on crossing brainstem fibers were conducted. For this the brainstem ROI was portioned horizontally into the left and right (division coordinate $x = 0$) and vertically into the pons and midbrain (division coordinate $z = -23$) (cp. Fig. 1d).

DTI preprocessing and analysis

This structural connectivity (Johansen-Berg and Rushworth 2009) was visualized by analyzing the main diffusion direction of water molecules by DTI. The data were preprocessed and analyzed with FMRIB's Diffusion Toolbox (FDT) as part of the FSL package (FSL v5.0, FDT v2.0, Oxford, UK). First, eddy current correction (Behrens et al. 2003a) and brain extraction (Smith 2002) were applied. DTIFIT first eigenvector was used to check for data quality. Then the local probability density function of a diffusion tensor model was calculated using an algorithm that models intravoxel crossing fibers (Behrens et al. 2007). Structural connectivity of the brainstem to the core region of the PIVC was determined using the connectivity-based seed classification option of the FSL probabilistic tractography software: number of samples = 5,000/voxel; curvature threshold = 0.2; number of steps = 2,000; step length = 0.5 mm (Behrens et al. 2003a, b). The brainstem including the left and right vestibular nuclei was the starting seed point, and the core region of the PIVC was used as the target region. A second analysis focused on the vestibular fibers crossing in the pons, the midbrain, the thalamus, or the corpus callosum.

fcMRI preprocessing and analysis

fcMRI assesses the spontaneous and functionally linked synchronicity of neuronal activity between anatomically distinct brain regions during a period of rest (Fox and Raichle 2007). This results in maps of so-called resting-state networks (RSN). All acquired images were preprocessed using the SPM8 software package (http://www.fil.ion.ucl.ac.uk/spm/software/spm8/), DARTEL (Diffeomorphic Anatomical Registration Through Exponentiated Lie Algebra; Ashburner 2007) and CONN functional connectivity toolbox v14 (Whitfield-Gabrieli and Nieto-Castanon 2012). Anatomical analyses in DARTEL included: (i) segmentation of the images into white matter (WM), gray matter (GM), and cerebrospinal fluid (CSF) using the New Segmentation algorithm implemented in SPM8 and including an intensity non-uniformity correction to account for smooth intensity variations caused by gradient distortions; (ii) applying the DARTEL approach for registration, normalization, and modulation; (iii) further normalization of the GM and WM images to MNI space and smoothing of the GM and WM images with a 4 mm full width at half maximum Gaussian kernel to increase signal to noise ratio. In the resulting images, each voxel represented an absolute amount of brain volume, equivalent to the brain volume per unit prior to normalization. Functional analyses in CONN included: (i) import of the preprocessed anatomical volumes; (ii) spatial preprocessing of functional volumes [slice-timing correction, realignment, normalization, and smoothing (4-mm FWHM Gaussian filter) using SPM8 default parameter choices]; (iii) nuisance regression using Compcor (control of physiological/movement confounds; Behzadi et al. 2007) and ART (artifact detection/scrubbing): time series characterizing the estimated subject motion (three rotation and three translation parameters, plus another six parameters representing their first-order temporal derivatives; cp. Fox et al. 2005) as well as the BOLD time series within the subject-specific white matter mask (three PCA parameters), CSF mask (three PCA parameters), a mask for the fourth ventricle, and the global signal were used as temporal covariates and removed from the BOLD functional data using linear regression; (iv) temporal preprocessing of the resulting residual BOLD time series using a band-pass filter ($0.008\ \text{Hz} < f < 0.09\ \text{Hz}$); (v) estimation of first-level functional connectivity (Pearsons' correlation) maps for each of the default Brodmann area seeds (located in the conn/rois folder) and the vestibular nuclei ROIs; and (vi) second-level seed-to-voxel connectivity mapping and ROI-to-ROI analyses. Furthermore, since head motion has recently been shown to differentially impact functional connectivity measures (Power et al. 2012; Van Dijk et al. 2012), the mean head motion was assessed as a potential confounding factor using FMRIB's Linear Image Registration Tool (MCFLIRT; Jenkinson et al. 2002). The mean head motion represents the mean absolute displacement (in mm) of each brain volume compared to the previous volume and was estimated from the translation parameters in x, y, and z directions across all time points.

Statistics and map display

Statistics were performed in FSL (DTI) and SPM (fcMRI). Analyses are reported according to Poldrack and colleagues (2008). The Conn toolbox uses topological false discovery rate (FDR) correction procedures (Cumbley et al. 2010, Benjamini and Hochberg 1995). ROI-to-ROI functional connectivity analyses are reported at $p < 0.05$ (FDR-corrected, two-sided). Seed-to-voxel functional connectivity analysis is reported at $p < 0.001$ (cluster-level statistics, FDR-corrected, one-sided). So as not to complicate the already complex results, we chose to focus on the positive contrasts. A participant was considered to have structural connections from the vestibular nuclei to the core region of the PIVC if any voxel in the vestibular nuclei passed a threshold of sending 1,500 of 5,000 (30 %) samples or

higher to the opercular–insular ROI (Putnam et al. 2010). Statistical maps were thresholded accordingly with the min (30 %) and max intensity (100 %). DTI and fcMRI maps were projected onto high-resolution T1-weighted default anatomical brain image distributed with Chris Rorden's MRIcron version 06-2013 (http://www.mricro.com). In case of the FSL, default atlases did not suffice for subanatomical details and we used superimposed slides of the "Olszewski and Baxter's Cytoarchitecture of the Human Brainstem" for structures in the brainstem (Büttner-Ennever and Horn 2014) and slides of the "Stereotactic Atlas of the Human Thalamus and Basal Ganglia" for the thalamus (Morel 2007).

Results

Handedness and integrity of vestibular function

The laterality quotient for right-handedness according to the 10-item inventory of the Edinburgh test was +100 % in 22 of the volunteers, +90 % in 1, and +80 % in another volunteer. Three of the 24 participants showed pathological tilts of the SVV ($n = 2$) or the VOR ($n = 1$) and thus had to be excluded from analysis. Therefore, 21 participants were included in the analyses as the study cohort. Head motion measured by the mean relative displacement (in mm) was low (0.06 ± 0.06).

Functional connectivity (seed-based fcMRI)

ROI-to-ROI analyses (cp. Fig. 2; Table 1) of the right vestibular nucleus (VN-R) showed functional connectivity ($p < 0.05$, FDR-corrected, T_{min} 2.66, two-sided, positive contrasts) to the left vestibular nucleus (VN-L), left and right insular cortex (BA 13), and the right posterior entorhinal cortex (BA 28). The VN-L ROI showed functional connectivity ($p < 0.05$, FDR-corrected, T_{min} 2.91, two-sided, positive contrasts) to the VN-R, left and right piriform cortex (BA 27), left and right insular cortex (BA 13), the right posterior entorhinal cortex (BA 28), and the right perirhinal cortex (BA 35). Both VN-R and VN-L had a high connectivity to each other, both insular cortices (re > li, BA 13), and the right posterior entorhinal cortex (BA 28). Additionally, VN-L projected to both piriform cortices (BA 27) and the right perirhinal cortex (BA 35). The right posterior entorhinal cortex (BA 28) includes the hippocampus.

Seed-to-voxel analysis (cp. Fig. 3b; Table 2) of the VN-R seed revealed functional connectivity ($p < 0.001$, cluster level statistics, FDR-corrected, k_{min} 510, one-sided, positive contrasts) to a bilateral cluster ($x = 8$, $y = -36$, $z = -32$; 12,562 voxels) and a left-sided cluster ($x = -42$, $y = -16$, $z = 0$; 510 voxels) covering BA-labeled cortical areas and not-BA-labeled subcortical area within the brainstem and cerebellum. The VN-L seed displayed functional connectivity ($p < 0.001$, cluster level statistics, FDR-corrected, k_{min} 348, one-sided, positive contrasts) to a bilateral cluster ($x = -8$, $y = -36$, $z = -32$; 16,810 voxels), two right-sided clusters ($x_1 = 44$, $y_1 = -10$, $z_1 = -6$ with 882 voxels; $x_2 = 26$, $y_2 = -32$, $z_2 = -6$ with 368 voxels) and a left-sided cluster ($x = -40$, $y = 8$, $z = -18$; 545 voxels) covering the BA-labeled cortical areas and not-BA-labeled subcortical area within the brainstem and cerebellum. Detailed information may be found in Table 2.

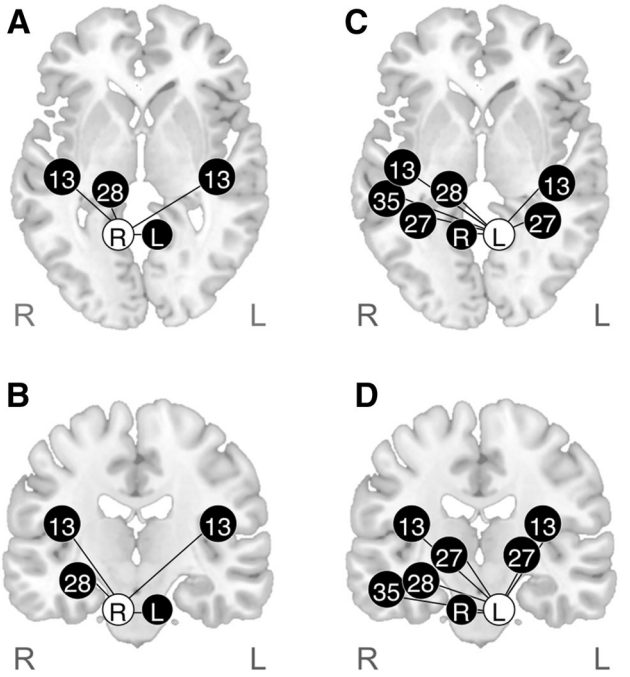

Fig. 2 fcMRI ROI-to-ROI analysis. **a** *White circle* characterizes the seed ROIs. *Black circles* characterize their functionally connected ROIs. **a**, **b** The functional connectivity of the right vestibular nucleus (VN-*R*), **c**, **d** the functional connectivity of the left vestibular nucleus (VN-*L*) in axial (*top row*) and coronal (*bottom row*) display. For purposes of clarity each ROI is identified by its approximal centroid position and attributed to a Brodmann area (indicated by *numbers*). Results were thresholded at FDR-corrected $p < 0.05$. Both vestibular nuclei had a high connectivity to each other, both insular cortices (re > li), and the right BA 28. Additionally, VN-L projected to both BA 27 and the right BA 35. Results are presented at $p < 0.05$ (FDR-corrected, two-sided, positive contrasts). *BA* Brodmann area, *BA* 13 insular cortex, *BA* 27 piriform cortex, *BA* 28 posterior entorhinal cortex, *BA* 35 perirhinal cortex, *VN*-R right vestibular nucleus, *VN*-L left vestibular nucleus

Structural connectivity (DTI tractography)

Probabilistic tractography of the vestibular nuclei to the PIVC (>30 % of samples) resulted in ipsilateral and contralateral projecting fibers (cp. Fig. 3a; Table 3).

Table 1 Overview of ROI-to-ROI functional connectivity

	ROI connection to	BA	H	T(20)	P-FDR	P-unc
NV-R	Vestibular nucleus		L	15.68	0.0000	0.0000
	Insular cortex	13	R	3.08	0.0210	0.0059
			L	2.66	0.0423	0.0151
	Posterior entorhinal cortex	28	R	3.03	0.0219	0.0066
NV-L	Vestibular nucleus		R	15.68	0.0000	0.0000
	Piriform cortex	27	R	3.66	0.0127	0.0015
			L	3.38	0.0178	0.0030
	Insular cortex	13	R	3.38	0.0178	0.0030
			L	2.91	0.0320	0.0087
	Posterior entorhinal cortex	28	R	3.16	0.0230	0.0050
	Perirhinal cortex	35	R	2.95	0.0314	0.0079

ROI-to-ROI functional connectivity was reported at 0.05 p-FDR, two-sided, positive contrasts. Vestibular nuclei had a high connectivity to each other, both insular cortices (BA 13), and the right posterior entorhinal cortex (BA 28). Additionally, VN-L projected to both piriform cortices (BA 27) and the right perirhinal cortex (BA 35). For visualization, please view Fig. 2

BA Brodmann area, *H* hemisphere, *VN-R* right vestibular nucleus, *VN-L* left vestibular nucleus

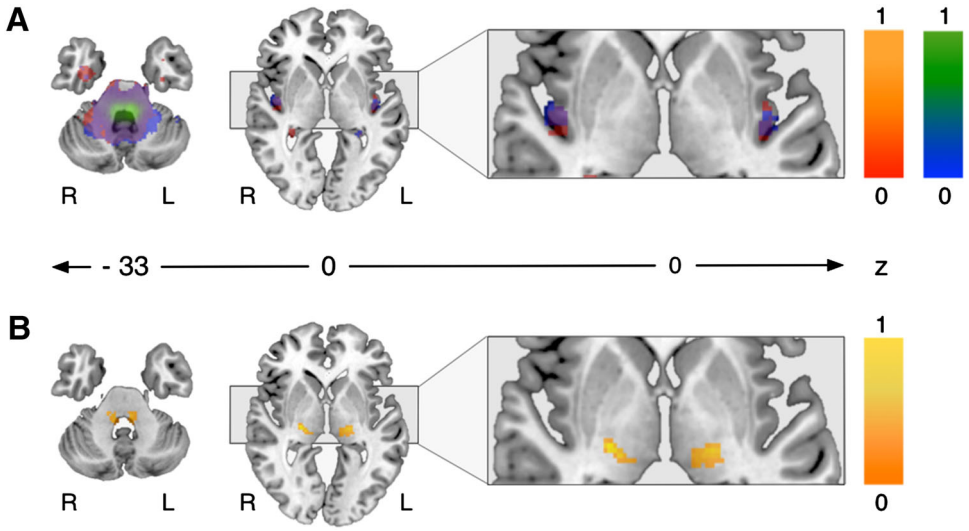

Fig. 3 Combined DTI and fcMRI analyses. Our results suggest congruence between functional **a** connectivity and structural **b** connectivity of the human vestibular system within a complex bilateral network, in which the parieto-insular vestibular cortex (PIVC) is a central cortical structure. DTI and fcMRI maps were thresholded to 0–1 of the maximally calculated probability value. **a** In the multivariate seed-to-voxel analysis, the vestibular nuclei on the right side (color coded from *red* to *yellow*) and left side (color coded from *blue* to *green*) show a significant functional connectivity to the core region of the PIVC (here long insular gyri IV and V). Please note *blue* and *red* areas in the PIVC bilaterally. Overlapping regions of left and right connectivities turn into green or violet, respectively. **b** At group level, the DTI tractography showed the most reliable structural connection ipsilateral between brainstem, thalamus, and the opercular–insular region (*yellow*)

Depending on the laterality, the affected structures and the level of crossing of five different vestibular brainstem pathways were identified—three ipsilateral non-crossing (cp. Fig. 4a–d i) and two crossing to the contralateral side (cp. Fig. 4a–d c). At the cortical level, the PIVCs were interhemispherically connected via the splenium of the corpus callosum (cp. Fig. 5). Involved anatomical structures were located at the level of the pons ($z = 33$), the midbrain ($z = -17$), and the thalamus ($z = 0$ and $z = 6$). Probabilistic tracts were quantified using waytotal, maximal intensity, and nonzero voxels (v). In this context waytotal (w) corresponds to the total number of generated tracts from each seed mask that reached at least one of the other masks and were not rejected by inclusion or exclusion mask criteria. Maximal intensity (mi) reflects the number of voxels in the seed times 5,000. Ipsilateral (i) pathways traveled through the thalamus or directly reached the insular–opercular ROI, bypassing the thalamus

Table 2 Overview of seed-to-voxel functional connectivity

Seed	Cluster	*x*, *y*, *z*	*K*	Cluster p-FDR	Cluster p-unc	H	Regions
NV-R	1	8, −36, −32	12,562	0.000000	0.000000	R/L	BA 28, 34, 35, 36, BA-not labeled
						R	BA 13, 20, 21, 27, 30, 37, 38, 44, 47
	2	−42, −16, 0	510	0.000052	0.000003	L	BA 13, 38, 47, 22, 28, BA-not labeled
NV-L	1	−8, −36, −32	16,810	0.000000	0.000000	R/L	BA 20, 21, 22, 28, 34, 35, 36, 38, BA-not labeled
						L	BA 27, 30
	2	44, −10, −6	882	0.000001	0.000000	R	BA 6, 13, 22, 38, 44, 47, BA-not labeled
	3	−40, 8, −18	545	0.000046	0.000003	L	BA 6, 13, 22, 38, 47, BA-not labeled
	4	26, −32, −6	368	0.000656	0.000055	R	BA 19, 27, 28, 29, 30, 35, 36, BA-not labeled

Seed-to-voxel functional connectivity was reported at cluster level statistics 0.001 p-FDR, one-sided, positive contrasts. For visualization please view Fig. 3b. Clusters covered BA-labeled cortical areas and BA-not labeled regions subcortical areas within the brainstem and cerebellum

BA Brodmann area, *BA* 6 premotor cortex, *BA* 13 insular cortex, *BA* 19 associative visual cortex, *BA* 20 inferior temporal gyrus, *BA* 21 middle temporal gyrus, *BA* 22 superior temporal gyrus, *BA* 27 piriform cortex, *BA* 28 posterior entorhinal cortex, *BA* 29 retrosplenial cingulate cortex, *BA* 30 cingulate cortex, *BA* 34 anterior entorhinal cortex, *BA* 35 perirhinal cortex, *BA* 36 parahippocampal cortex, *BA* 37 fusiform gyrus, *BA* 38 temporopolar area, *BA* 44 inferior parietal cortex, pars opercularis, *BA* 47 inferior prefrontal gyrus, *VN-R* right vestibular nucleus, *VN-L* left vestibular nucleus

Table 3 Overview of DTI tractography structural connectivity

	NV	Pons	Mesencephalon	Thalamus, posterolateral	Thalamus, paramedian
Ipsilateral and direct	**i**	**MVN, PCR, ML, SEL**	**MRF, MRFv, ML, SNc,**	**(IC)**	
Ipsilateral and indirect	**i**	**MVN, PCR, ML, SEL**	**MRF, MRFv, PAGl, PPTd, SC,**	**LP, VPLp, Pu (A-L-M), Po, R**	**CL, CM**
Pontine crossing	**i**	**NVIII, LVN, ML, PN**			
	c	*NVIII, LVN, ML, Gi, MSO, LSO, POC*	*ML, MRF, BIC*	*Pu (A, **M**), R, VPLp, IC*	
Mesencephalic crossing	**i**	**MLF, PGiD**	**MLF, III**		
	c		*MLF, III, SCP, CLi*	*Pu (**A**, M), LP, VPLp/v, VPM, IC, R, Zi*	

DTI probabilistic tractography structural connectivity was reported at a threshold of sending 1,500 of 5,000 (30 %) samples or higher from the vestibular nuclei (=seed) to the parieto-insular vestibular cortex (PIVC = target). Note that this table was divided as to laterality into ipsilateral (i, bold) and contralateral pathways (c, italic). For visualization of the pathways please view Fig. 4

III oculomotor nucleus, *BIC* brachium of the inferior colliculus, *CL* central lateral nucleus (posterior part), *CLi* caudal linear nucleus, *CM* centromedian nucleus, *Gi* gigantocellular nucleus, *IC* internal capsule, *LP* lateral posterior nucleus, *LSO* lateral superior olivary nucleus, *LVN* lateral vestibular nucleus, *MVN* medial vestibular nucleus, *ML* medial lemniscus, *MLF* medial longitudinal fascicle, *MRF* mesencephalic longitudinal formation, *MRFv* mesencephalic longitudinal formation, ventral part, *MSO* medial superior olivary nucleus, *NV*III vestibular nerve, *PAG*l periaqueductal gray, lateral part, *PCR* parvocellular reticular nucleus, *PGiD* dorsal paragigantocellular nucleus, *PIVC* parieto-insular vestibular cortex, *Po* Posterior nucleus, *PN* pontine nuclei, *POC* periolivary complex, *PPTd* pedunculopontine nucleus, pars dissipata, *PuA* anterior pulvinar, *PuM* medial pulvinar, *PuL* lateral pulvinar, *R* reticular thalamic nucleus, *SC* superior colliculus, *SCP* superior cerebellar peduncle, *SEL* subependymal layer, *SNc* substantia nigra, pars compacta (ventral tier pars α and dorsal tier pars β), *VN* Vestibular nucleus, *VPLp* ventral posterior lateral nucleus, *VPLv* ventral posterior lateral nucleus (posterior and anterior divisions), *VPM* ventral posterior medial nucleus, *Zi* zona incerta

(cp. Fig. 4 a–d i). The first tract was called "ipsilateral and direct" (cp. Fig. 4a–d i, pink). In detail, this tract (R: (*w*) = 629.1 ± 743.2; (mi) = 481.2 ± 601.3; (*v*) = 14,379.0 ± 632.4, L: *w* = 614.7 ± 1,206.3; mi = 488.9 ± 957.5; *v* = 7,971.8 ± 6,446.9) coursed through the dorsomedial part of the pons [more precisely, the medial vestibular nucleus (MVN), parvocellular reticular nucleus (PCR), medial lemniscus (ML), subependymal layer (SEL)] and the lateral part of the midbrain [mesencephalic longitudinal formation (MRF), ML, the pars compacta of the substantia nigra (SNc)] and projected to the ipsilateral region of the PIVC via the internal capsule (IC). The second tract was called "ipsilateral and indirect" (cp. Fig. 4 a–d i, yellow). In detail, this tract (R: *w* = 6,037.6 ± 5,725.4; mi = 3,368.1 ± 2,868.2; *v* = 12,795.8 ± 7,289.4, L: *w* = 36,827.8 ± 17,462.6; mi = 15,056.5 ± 7,519.7; *v* = 105,785.9 ± 26,480.3) coursed through the dorsomedial part of the pons (MVN,

PCR, ML, SEL) and the dorsolateral part of the midbrain [MRF, MRFv, lateral part of the periaqueductal gray (PAGl), pars dissipata of the pedunculopontine nucleus (PPTd), superior colliculus (SC)]. From there, it projected to the ipsilateral region of the PIVC via both the posterolateral thalamus [lateral posterior nucleus (LP), ventral posterior lateral nucleus (VPLp), the posterior nucleus (Po), and the anterior, medial, or lateral pulvinar (PuA,L,M)] and the paramedian thalamus [posterior part of the central lateral nucleus (CL), centromedian nucleus (CM)].

Contralateral (C) pathways crossed at the level of the pons and the mesencephalon (cp. Fig. 4a–d c). The third tract was called "pontine crossing" (cp. Fig. 4a–d c, blue). In detail, this tract (L: $w = 115.4 \pm 215.4$; mi $= 77.6 \pm 157.2$; $v = 9{,}932.2 \pm 6{,}496.1$, R: $w = 264.9 \pm 304.2$; mi $= 120.4 \pm 139.5$; $v = 17{,}924.2 \pm 8{,}856.5$) coursed through the dorsolateral part of the ipsilateral [vestibular nerve (NVIII), lateral vestibular nucleus (LVN), ML, pontine nuclei (PN)] and contralateral pons [NVIII, LVN, ML, gigantocellular nucleus (Gi), medial superior olivary nucleus (MSO), lateral superior olivary nucleus (LSO), periolivary complex (POC)] and the lateral part of the contralateral midbrain [ML, MRF, brachium of the inferior colliculus (BIC)] and projected to the contralateral region of the PIVC via the posterolateral thalamus [Pu (A, M), Rt, VPLp] and IC. The fourth tract was called "mesencephalic crossing" (cp. Fig. 4a–d c, green). In detail, this tract (L: $w = 5.2 \pm 5.1$; mi $= 3.4 \pm 2.9$; $v = 2{,}248.8 \pm 1{,}891.0$, R: $w = 63.6 \pm 80.5$; mi $= 36.2 \pm 957.5$; $v = 14{,}084.2 \pm 9{,}607.5$) coursed through the mediodorsal part of the pons [MLF, dorsal paragigantocellular nucleus (PGiD)] and the medial part of the ipsilateral midbrain [MLF, oculomotor nucleus (III)] and contralateral [MLF, III, superior cerebellar peduncle (SCP), caudal linear nucleus (CLi)] and projected to the contralateral PIVC via the posterolateral thalamus [Pu (A, M), LP, VPLp, ventral posterior lateral nucleus (posterior and anterior divisions, VPLv), ventral posterior medial nucleus (VPM), R, zona incerta (Zi)] and the IC.

Furthermore, we found adjacent connections at the level of the VN and PIVCs. Vestibular nuclei were connected via internuclear tracts (L: $w = 47{,}391.1 \pm 47{,}380.8$; mi $= 11{,}839.8 \pm 9{,}346.1$; $v = 1{,}767.6 \pm 552.6$, R: $w = 94{,}095.8 \pm 61{,}409.8$; mi $= 16{,}572.6 \pm 8{,}021.9$; $v = 2{,}714.3 \pm 768.4$). Both PIVC were connected via interhemispherical tracts (L: $w = 18.9 \pm 29.7$; mi $= 11.8 \pm 18.2$; $v = 4{,}393.9 \pm 4{,}508.8$, R: $w = 256.1 \pm 402.5$; mi $= 112.6 \pm 179.4$; $v = 29{,}697.1 \pm 18{,}560.3$) and projected through the antero-caudal splenium of the corpus callosum (cp. Fig. 5). FcMRI and DTI parameters did not correlate significantly.

Discussion

Our in vivo investigation of vestibular connectivity by means of combined structural and functional connectivity mapping found a congruent functional and structural link between the vestibular nuclei in the pontomedullary brainstem and the ipsilateral and contralateral vestibular cortex. In the cortex, the ROI focused on the core region of the parieto-insular vestibular cortex (PIVC) in the opercular–insular region (cp. Fig. 6). Interconnecting fiber tracts could be delineated between the vestibular nuclei at the pontomedullary level. From the vestibular nuclei, five separate and distinct vestibular brainstem pathways were identified (cp. Fig. 7). Three of these run ipsilaterally without crossing the midline, while the other two cross either at the level of the pons or midbrain to continue traveling contralaterally. The ipsilateral pathways run through either the posterolateral or the paramedian thalamus or directly contact an area of the insula inferior and anterior to the PIVC. Both the contralateral pathways run through the posterolateral thalamus to the vestibular cortex. The PIVCs of the right and left hemispheres are connected transcallosally through the antero-caudal splenium. In addition to the known interconnection between the vestibular nuclei, our study revealed two more brainstem crossings of the bilaterally organized vestibular circuitry. Thus, the three crossings are located (1) at the level of the vestibular nuclei, (2) at the pontine level above the vestibular nuclei, and (3) at the mesencephalic level. The fourth crossing travels transcallosally between the vestibular cortex areas of both hemispheres. The basic network of the entire bilateral central system is best visualized by a "vestibular rope ladder".

Five ascending vestibular pathways from brainstem to cortex

Our findings are in line with previous human and animal studies that examined parts of the pathways, but not the entire system. On the evidence of tracer studies primarily in the cat and macaque monkey, vestibular pathways course bilaterally from the vestibular nuclei through at least four ascending tracts such as the MLF (Uchino et al. 1981; Graf and Ezure 1986; Büttner-Ennever 1992), the ascending Deiters' tract (crossed and uncrossed) (Maciewicz et al. 1982), the crossed ventral tegmental tract (Lang et al. 1979), and the brachium conjunctivum to the ocular motor nuclei and the supranuclear integration centers in the rostral mesencephalic brainstem (Büttner-Ennever 1999). Lesion studies and functional imaging point toward a comparable network of vestibular pathways in humans within the brainstem. Vestibular eye–head coordination in the roll plane is thought to be mainly mediated by crossed

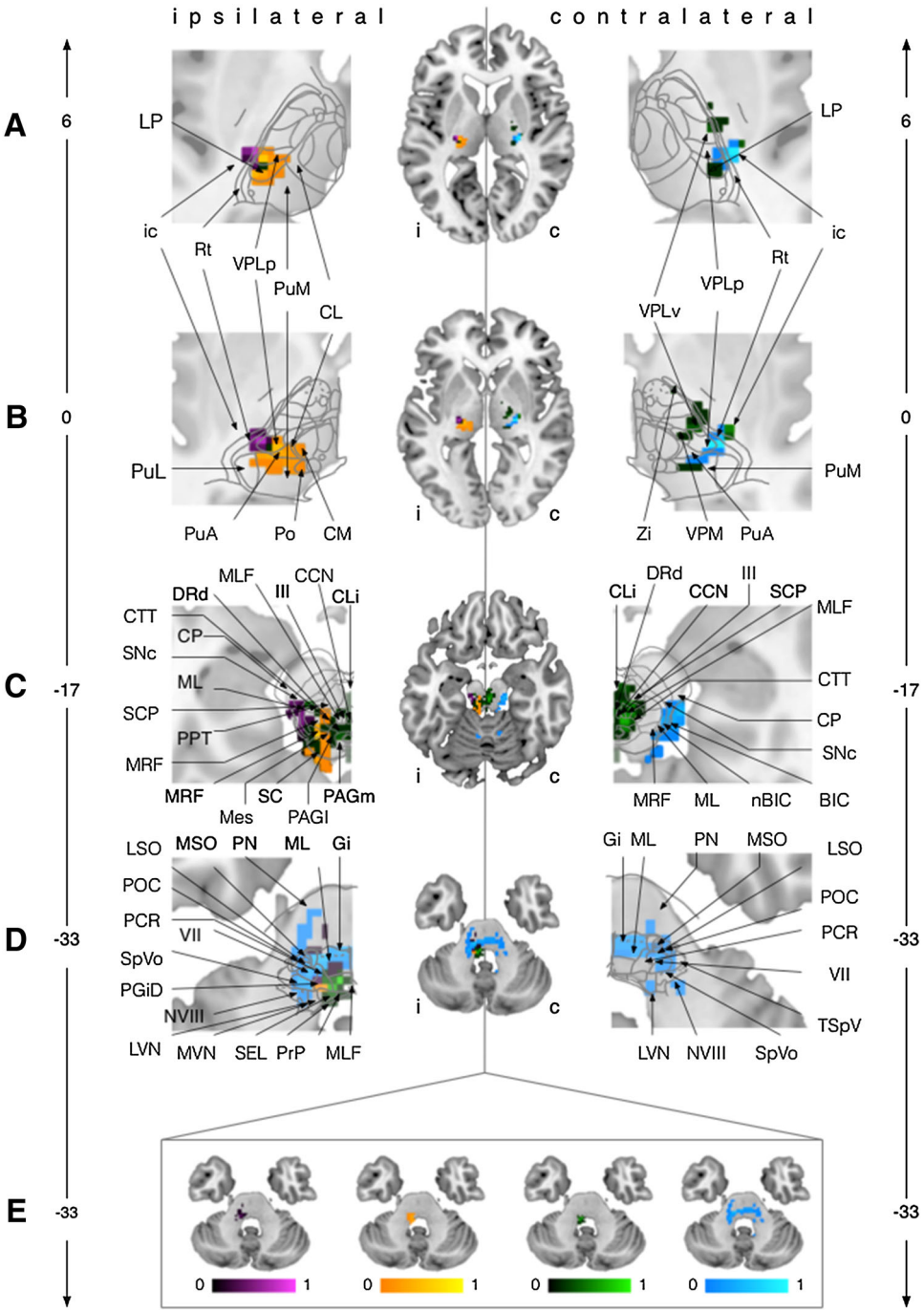
ipsilateral
contralateral
A
B
C
D
E
6
0
-17
-33
LP
ic
Rt
VPLp
PuM
CL
PuL
PuA
Po
CM
VPLv
Zi
VPM
MLF
CCN
DRd
III
CLi
CTT
CP
SNc
ML
SCP
PPT
MRF
SC
PAGm
Mes
PAGl
SCP
nBIC
BIC
LSO
MSO
PN
Gi
POC
PCR
VII
SpVo
PGiD
NVIII
LVN
MVN
SEL
PrP
TSpV
i
c
0
1

◀**Fig. 4** Structural vestibular connectivity of the human brainstem and thalamus. Here, the major findings of the DTI tractography are visualized. Note that the brain slides are divided into ipsilateral pathways (*i*, *left*) and contralateral pathways (*c*, *right*). To clarify the subcortical anatomical details, slides of the "Olszewski and Baxter's cytoarchitecture of the Human Brainstem" for structures in the brainstem (Büttner-Ennever and Horn 2014) and slides of the "Stereotactic Atlas of the Human Thalamus and Basal Ganglia" for structures within the thalamus (Morel 2007) were overlayed. They were then placed over high-resolution T1-weighted brain slides on each side. **a**, **b** Slides of the thalamus (MNI $z = 6$ overlayed with slide D6.3, MNI $z = 0$ overlayed with slide D0.9). **c**, **d** Slides of the brainstem (MNI $z = -17$ overlayed with cross section 401 and MNI $z = -33$ overlayed with cross section 1501). **e** The pathways individually with their respective color code according to their characteristics (*pink* ipsilateral and direct, *yellow* ipsilateral and indirect, *blue* pontine crossing to the contralateral side, *green* mesencephalic crossing to the contralateral side). *Maps* were thresholded to 0–1 of the maximally calculated probability value. For a concise overview of these results, view Table 3. **a**, **b** *CL* central lateral nucleus (posterior part), *CM* centre médian nucleus (or *centromedian*), *IC* internal capsule, *LP* lateral posterior nucleus, *Po* posterior nucleus, *PuA* anterior pulvinar, *PuM* medial pulvinar, *PuL* lateral pulvinar, *Rt* reticular thalamic nucleus, *VPLP* ventral posterior lateral nucleus (posterior and anterior divisions), *VPLv* ventral posterior lateral nucleus (posterior and anterior divisions), *VPM* ventral posterior medial nucleus, *Zi* zona incerta. **c** III oculomotor nucleus, *BIC* brachium of the inferior colliculus, *CCN* central caudal nucleus, *CCT* cerebellothalamic tractotomy, *CLi* caudal linear nucleus, *CP* cerebral peduncle, *DRd* dorsal raphe nucleus, dorsal part, *MesV* mesencephalic trigeminal nucleus, *ML* medial lemniscus, *MLF* medial longitudinal fascicle, *MRF* mesencephalic longitudinal formation, *MRFv* mesencephalic longitudinal formation, *ventral* part, *nBIC* nucleus of the brachium of the inferior colliculus, *PAGl* periaqueductal gray, *lateral* part, *PAGm* periaqueductal gray, *medial* part, *PPTd* pedunculopontine nucleus, pars dissipata, *SC* superior colliculus, *SCP* superior cerebellar peduncle, *SNc* substantia nigra, pars compacta (ventral tier pars α and dorsal tier pars β). **d** VII facial nucleus; *Gi* gigantocellular nucleus, *LSO* lateral superior olivary nucleus, *LVN* lateral vestibular nucleus, *ML* medial lemniscus, *MLF* medial longitudinal fascicle, *MSO* medial superior olivary nucleus, *MVN* medial vestibular nucleus, *N*VIII vestibular nerve, *PCR* parvocellular reticular nucleus, *PGiD* dorsal paragigantocellular nucleus, *PN* pontine nuclei, *POC* periolivary complex, *PrP* prepositus nucleus, *SEL* subependymal layer, *SpVo* spinal trigeminal nucleus, oral part, *TSpV* spinal trigeminal tract

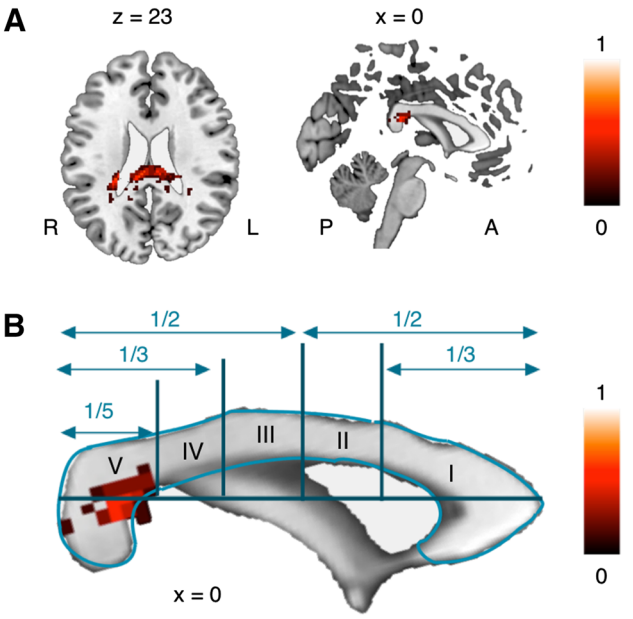

Fig. 5 Interhemispherical DTI tractography analysis. Interhemispheric tracts between the core region PIVC projected through the antero-caudal splenium of the corpus callosum, region V, following the Witelson classification. **a** The interhemispheric tract in an axial ($z = 23$) and sagittal slide ($x = 0$). **b** The projected Witelson classification on an enlarged corpus callosum of a high-resolution T1-weighted default anatomical brain image

projections running via the MLF to the contralateral interstitial nucleus of Cajal (INC) (Dieterich and Brandt 1993a), which represents the integration center for the eye, head, and body movements in the roll and pitch planes (Büttner-Ennever 1999; Straka and Dieringer 2004). The contralateral pathways crossing in the mesencephalon or pons in our study might represent these projections. However, at this stage it is difficult to distinguish MLF, crossed ventral tegmental tract, ascending Deiters' tract, or brachium conjunctivum. In addition, an ipsilateral vestibulo-thalamic tract (IVTT) was described in patients with acute unilateral anteromedial pontomesencephalic infarctions that caused ipsilateral tilts of the subjective vertical (Zwergal et al. 2008). This tract is obviously responsible for perceptual information on verticality and is located in the medial portion of the medial lemniscus. Its existence was subsequently confirmed by a re-analysis of an anterograde tracer labeling study in the non-human primate (Zwergal et al. 2008). We did not find a paramedian ipsilateral pathway in our data. However, in another study where the target was the striatum, we were able to do so (unpublished data). An H_2O^{15}-PET study during caloric stimulation of the right and left horizontal semicircular canals suggested uncrossed ascending projections, owing to the predominance of activation patterns in the ipsilateral opercular–insular cortex (Dieterich et al. 2003). In our current study, the ipsilateral pathways might represent these projections and probably correspond to the ascending Deiters' tract found in animal data. Another H_2O^{15}-PET study, which used the same paradigm in patients with strategic lesions along the vestibular pathways through the posterolateral thalamus also suggested (i) crossed and uncrossed ascending projections, (ii) a passage of the very same projections through the posterolateral thalamus ("indirect ipsilateral pathway"), and (iii) a direct projection to the inferior part of the insula ("direct ipsilateral pathway"), bypassing the vestibular relay station in the posterolateral thalamus regions (Dieterich et al. 2005). However, the existence and course of these projections as

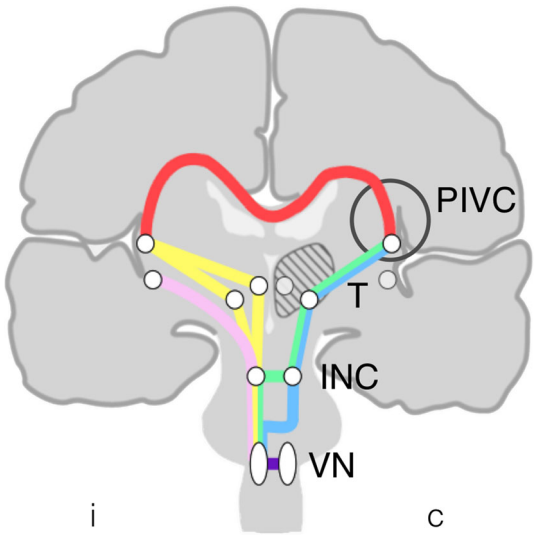

Fig. 6 Schematic overview of the vestibular rope ladder system. The basic network of the vestibular system is best visualized as a rope ladder. We focused on the core region of the parieto-insular vestibular cortex (PIVC) in the opercular–insular region and identified five separate and distinct vestibular brainstem pathways. Three of these run ipsilaterally (i) without crossing the midline, while the other two crossed either on the level of the pons (*blue*) or midbrain (*green*) to continue traveling contralaterally (**c**). The ipsilateral pathways run through either the posterolateral or the paramedian thalamus (*T*, *yellow*) or directly (*pink*) contact an area of the insula inferior anterior to the PIVC. Both contralateral pathways run through the posterolateral thalamus to the vestibular cortex. Our study revealed three brainstem crossings of the bilaterally organized vestibular circuitry. These are located (1) at the level of the vestibular nuclei (VN), (2) at the pontine level above the vestibular nuclei, and (3) at the mesencephalic level with the interstitial nucleus of Cajal (INC) as the crucial structure. The fourth crossing travels transcallosally between the vestibular cortex areas of both hemispheres

proposed by the patient studies up to now had not been confirmed by direct verification. The latter direct projection bypassing the thalamus is supported by earlier electrophysiological and tracer studies in the cat (Blum et al. 1979a, b). The tracer labeled not only neurons in the ventral posterolateral thalamic nucleus, but also neurons directly adjacent although outside the thalamus. In both locations, short-latency (<3.5 ms), large-amplitude-evoked potentials from vestibular nerve stimulation and antidromic field potentials from cortical stimulation of vestibular areas were recorded (Blum et al. 1979a). This indicates that these neurons relay vestibular activity directly to vestibular cortex areas at short latency, probably via an ascending disynaptic pathway.

What is the functional meaning of a "vestibular rope ladder system" with several crossings of vestibular pathways at different levels?

The question arises as to the different functions of the brainstem crossings at different levels. The interaction between the two vestibular nuclei (Büttner-Ennever 1992; Dieringer 1995; Straka and Dieringer 2004) allows the system to adjust both nuclei if one labyrinth or one nerve is stimulated or lesioned, i.e., it permits a compensation for a tone imbalance. Second-order neurons in the vestibular nuclei also receive and integrate vestibular input with sensory input of other modalities. This does not necessarily mean that both vestibular nuclei contain exactly the same information. Further, the ascending output from each vestibular nucleus is projected predominantly ipsilaterally and less contralaterally via the second pontine crossing.

The second crossing has been demonstrated in patients with brainstem infarctions who presented with graviceptive dysfunctions such as tilts of the perceived vertical, skew torsion of the eyes, and head tilt (Dieterich and Brandt 1993a). Together these dysfunctions form the so-called synkinesis of ocular tilt reaction as described in monkeys (Westheimer and Blair 1975). Unilateral lesions at the pontomedullary level cause ipsiversive tilts, whereas unilateral lesions at the pontomesencephalic level cause contraversive tilts (Dieterich and Brandt 1993a; Brandt and Dieterich 1994). This was recently confirmed by an analysis using voxelwise lesion behavior mapping (VLBM) in unilateral brainstem infarctions (Baier et al. 2012). Thus, this crossing is involved in eye–head coordination in the roll plane ("ascending OTR"; Brandt and Dieterich 1998).

The third crossing at the midbrain tegmentum occurs at the level of the INC, a region known to integrate velocity with position of eye–head movements in the vertical pitch and roll planes (Robinson et al. 1994; Büttner-Ennever 1999). A part of this complex is also the oculomotor nucleus, which contains paired and—around midline—unpaired areas. Here, the ascending vestibular input from both vestibular nerves is required to generate the descending motor output to coordinate the eye and neck muscles for orienting movements. This is mediated by a distributed tectoreticular system. The midbrain center not only integrates eye and head velocity into position (for holding the assumed eye–head position in space at the end of the movement), but also adjusts vestibular reflex responses to voluntary cortical control (Dieterich and Brandt 1993b; Brandt and Dieterich 1998). Long descending neurons called tecto-reticulo-spinal neurons mediate the process (Berthoz and Grantyn 1986): They originate in the INC, run through the MLF (Fukushima et al. 1987) to the pontine level, and couple eye and head roll motion by excitatory ipsilateral connections with complex axonal branching. In brief, the above-described functions of the crossing within the INC–oculomotor nucleus-midbrain center require multisensory and motor pathways for eye–head coordination. VLBM analysis also found this area in patients with unilateral brainstem infarctions who presented with contralateral tilts of verticality (Baier et al. 2012).

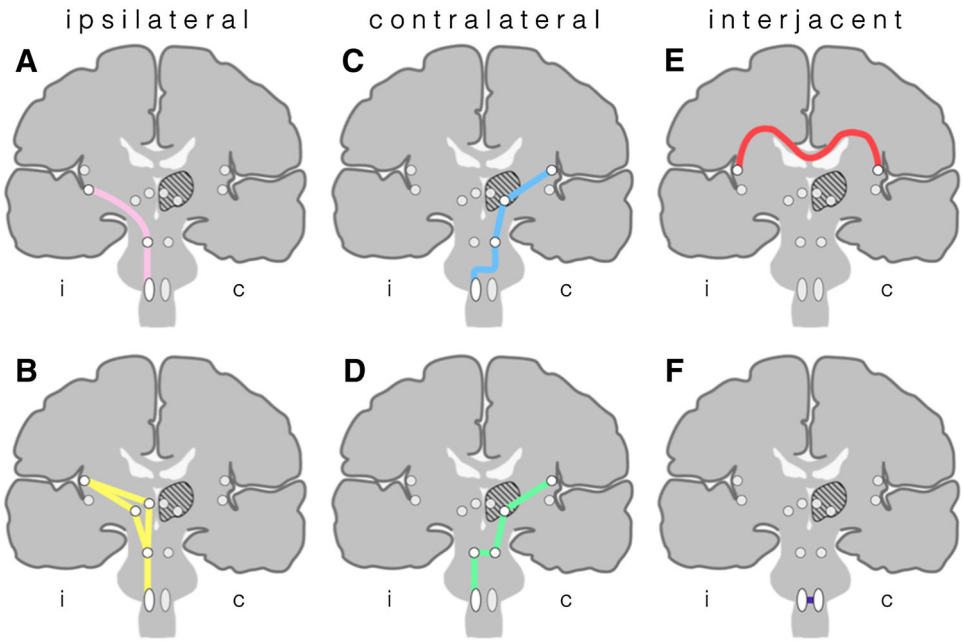

Fig. 7 Schematic overview of the vestibular pathways within the brainstem. Vestibular pathways project from the vestibular nucleus bilaterally, ipsi-(i) and contralaterally (**c**) to the parieto-insular vestibular cortex (PIVC). **a**, **b** Ipsilateral pathways (direct without relay stations within the thalamus = *pink*, indirect with paramedian and posterolateral relay stations within the thalamus = *yellow*), **c**, **d** Contralateral pathways (with pontine crossing = *blue*, with mesencephalic crossing = *green*), and **e**, **f** adjacent pathways of the PIVC in the antero-caudal splenium of the corpus callosum (**e** in *red*) or vestibular nuclei (**f** in *purple*). Since the vestibular nuclei were chosen as the seed regions, the well-known interconnections between both nuclei were not traced. However, they are included in the schematic drawings as the first crossing

It is remarkable that no crossing between the vestibular thalamic structures is known. The functions of these structures appear to integrate multisensory input and project to the (multisensory) vestibular cortex areas ipsilaterally. Cross talk between the two hemispheres at the cortical level, however, is a precondition for a unique perception of position and motion of the body in space. This might be provided by the fourth "transcallosal" crossing which in the current study runs through the antero-caudal splenium of the corpus callosum. According to the Witelson's scheme for the topography of the midsagittal corpus callosum of the human adult, the fibers in our study were located in the most posterior part V, the splenium (Witelson 1989). Fibers of this part are known to project into/from the parietal, occipital, and temporal lobes (Hofer and Frahm 2006).

Earlier studies indeed suspected that there were projections between both hemispheres. Connections were proposed to exist, for example, between both temporo-occipital areas to represent the motion-sensitive area MT/V5, MST in animals (Maunsell and Newsome 1987) and in humans (Brandt et al. 1998; Becker et al. 2013). The studies available so far allow the assumption that transcallosal vestibular and (motion-sensitive) visual pathways run adjacent via the posterior part of the callosal fibers, through the region V of the corpus callosum (Fig. 5). The same is true for the interhemispheric connections of the somatosensory system. The traced area of the region V in the current study is known to contain fibers to/from the parietal and occipital cortex, but especially the temporal cortex regions.

Contrary to the primary somatosensory system, in which the hemispheres may simultaneously perceive different stimuli, the vestibular percepts of body orientation and motion have to be adjusted to a unique percept. Both hemispheres cannot perceive different body positions or movements at the same time. With respect to this function, the vestibular dominance of the non-dominant hemisphere (Dieterich et al. 2003) may provide the more reliable sensorial weight in cases of incongruent information in both hemispheres. The dominance of the vestibular cortex areas within the right hemisphere in right-handers and of those in the left hemisphere in left-handers has been repeatedly demonstrated (Dieterich et al. 2003; Janzen et al. 2008; zu Eulenburg et al. 2012).

The opercular–insular cortex as a "core region" within the vestibular cortical network

The congruence between structural and functional connectivity of the human vestibular system within a complex bilateral network also holds for our seed region, the

parieto-insular vestibular cortex (PIVC). Four of the five brainstem pathways link the vestibular nuclei with this region. The human PIVC is located in the posterior parietal operculum/retroinsular region and extends into the posterior parts of the insular lobe (zu Eulenburg et al 2012; Eickhoff et al. 2006b) on anatomical analogy to animal studies on macaques (Akbarian et al. 1993; Guldin and Grüsser 1998; Chen et al. 2010, 2011a). Compared to the ventral intraparietal area (VIP) and the medial superior temporal area (MSTd) in the macaque monkeys, the PIVC showed spatiotemporal characteristics in electrophysiological cortical registration that represented a gradual transformation of temporal responses suggesting a hierarchy in cortical vestibular processing, with the PIVC being most proximal to the vestibular periphery and MSTd being most distal (Chen et al. 2011b). This region seems to be the human homolog of the PIVC, which was defined in monkeys as a core region within a vestibular cortical network (Brandt and Dieterich 1994, 1999; Dieterich 2007; Lopez and Blanke 2011; zu Eulenburg et al. 2012). Our data further support the results of earlier functional imaging studies of multisensory vestibular cortical areas in humans using vestibular, somatosensory, and visual optokinetic stimulation (vestibular: Bucher et al. 1998; Bense et al. 2001; Fasold et al. 2002; Emri et al. 2003; somatosensory: Baumgartner et al. 2010; Bingel et al. 2004; visual: Dieterich et al. 1998; Konen and Kastner 2008). Within the multiple multisensory vestibular cortical areas such as the superior temporal gyrus, anterior insula, and adjacent inferior frontal gyrus, inferior parietal lobule, anterior cingulum, hippocampus, the PIVC is recognized to be the central area also in humans (Brandt et al. 1998; Dieterich and Brandt 2008; zu Eulenburg et al. 2012). The results of our ROI-to-ROI analyses confirmed the above-described dominance of the vestibular cortex of the non-dominant hemisphere, here the right one in right-handers. The current study was intentionally performed on right-handed subjects only because of these hemispherical dominances.

The single cortical area connected by fibers bypassing the thalamus corresponds best to a region found earlier in patients with posterolateral thalamic infarctions. This region was the only one in the ipsilateral hemisphere of these patients that was activated by caloric irrigation in an H_2O^5-PET study (Dieterich et al. 2005). All other projections to the temporo-parietal cortex ipsilateral to the lesion, including the PIVC, were not activated. It must be assumed that this direct extrathalamic connection provides a particular perceptual vestibular function. One can speculate that this is the human homolog of a rapid three-neuronal ascending tract found earlier in tracer and electrophysiological studies of cats (Blum et al. 1979a, b). In those latter animal studies, the labeled neurons were not only located in the lateral thalamic subnuclei VPL, VPM, and VL, but were also directly adjacent outside the thalamic nuclei.

Multiple vestibular relay stations in the thalamus

The traditional view that the posterolateral thalamic nuclei are the major and only relay stations of vestibular input to the cortex has to be corrected. Tracer and electrophysiological animals studies detected more than ten regions within the thalamus, which have been attributed to vestibular processing (Lopez and Blanke 2011). Our data reveal that regions in both the posterolateral (crossed and uncrossed projections) and paramedian (uncrossed projections) thalamus serve as vestibular relay stations for brainstem projections to (or from) the vestibular cortex. Since the method used in our study does not allow us to distinguish ascending from descending fibers, the projections may also run from the cortex to the thalamus or may be part of a thalamo-cortical loop as was described earlier for body movement control by Alexander et al. (1990).

The involvement of the posterolateral thalamus was first determined by vestibular stimulation in animal experiments of different species (Sans et al. 1970; Deecke et al. 1973; Büttner and Henn 1976; Lang et al. 1979; Asanuma et al. 1983; Shiroyama et al. 1999). These agree with findings in patients with ischemic posterolateral thalamic lesions (Dieterich and Brandt 1993b; Dieterich et al. 2005; Lee et al. 2005). The ventrolateral parts of the thalamus receive signals from the superior and medial vestibular nucleus (Shiroyama et al. 1999) and the contralateral half of the cerebellum via the superior cerebellar peduncle as well as the ipsilateral globus pallidus (Hyam et al. 2012). Nearly all these tracts project to the motor cortex (Hyam et al. 2012).

It is remarkable that patients with acute posterolateral thalamic infarctions only presented with tilts of the perceived subjective visual vertical (SVV), but not with eye–head tilts (i.e., no skew deviation, no ocular tilt reaction), which are mediated by ponto-mesencephalic brainstem structures (Dieterich and Brandt 1993b; Brandt and Dieterich 1994). The first description of SVV tilts in posterolateral thalamic infarctions showed ipsilateral as well as contralateral deviations (Dieterich and Brandt 1993b), thus confirming the "historical" thalamic stimulation experiments in humans by Hassler in 1959 and Tasker and co-workers in 1982 (Hassler 1959; Tasker et al. 1982). Electrical stimulation of the human Vim elicited a rotation or spinning of the body and head, either counterclockwise (more often) or clockwise (Tasker et al. 1982; Hawrylyshyn et al., 1978). The role of the ventrolateral thalamus for the modulation of graviceptive information was also confirmed by thalamic deep brain stimulation of the nucleus ventralis intermedius (Vim) in patients with medically

intractable tremor who presented with contralateral SVV tilts during the off phases of stimulation (Conrad et al. 2014). This Vim stimulation in tremor patients could be related to a decrease in the regional blood flow in vestibular cortical regions such as the retroinsular cortex and superior temporal gyrus (PET: Ceballos-Baumann et al. 2001). This also points to an interaction of Vim stimulation on vestibular thalamic signal processing.

The involvement of the paramedian thalamus as a vestibular relay station has been less often established in clinical studies (Dieterich and Brandt 1993b; Elwischger et al. 2012). The clinical characteristics of thalamic astasia fulfill the criteria of a central vestibular tone imbalance in the roll plane (Dieterich and Brandt 1993b). First descriptions of thalamic astasia were based on unilateral thalamic lesions, which included the posterolateral nuclei (Masdeu and Gorelick 1988). In a recent case report, thalamic astasia associated with contralesional tilts of the SVV was reported in a patient with a small-circumscribed paramedian infarction (Elwischger et al. 2012). An analysis applying VBLM techniques in 37 patients with thalamic infarctions and tilts of SVV identified two distinct anatomical sites that affect the processing of graviceptive signals at the thalamic level (Conrad et al. 2014): Contraversive SVV tilts were associated with dorsolateral and dorsomedial subnuclei lesions (VPLp, VPLv, CL, nucleus parafascicularis thalami, CM, parts of the VPM, Po and CL). The novel finding was that regions associated with ipsiversive SVV tilts were located lower and medial (nucleus endymalis thalami, the lower part of the nucleus parafascicularis, and the nucleus ruber tegmenti bordering the brachium conjunctivum). The uncrosssed and crossed vestibular pathways of our current study appear to run through these regions, though confirmation is necessary. The paramedian subnuclei (centromedian–parafascicular nucleus complex) in animal studies (rats) receive vestibular afferents mainly from the medial, superior, and inferior vestibular nuclei—with an ipsilateral predominance (Shiroyama et al. 1999)—and relay it to the lateral striatum (Schlag and Schlag-Ray 1984). The centromedian nucleus (CM) receives major afferents from cortical motor areas (Akert and Hartmann-von Monakow 1980), the medial pallidal segment (Kim et al. 1976), brainstem and thalamic reticular areas (McGuinness and Krauthammer 1980; Kayahara et al. 1994), and the vestibular nuclei. In addition, the CM plays a role in striatal activation and also participates in specific functions such as gaze control or initiation of visually guided movements (Schlag and Schlag-Ray 1984). These findings suggest a vestibular influence on the motor loop of the basal ganglia–thalamocortical projections.

Methodological limitations

There are several methodical limitations in our study that need to be taken into account in the interpretation of the data. One is in the method we used to ascertain the structural connectivity (Dauguet et al. 2007; Johansen-Berg and Rushworth 2009). DTI tractography has limited resolution ($2.0 \times 2.0 \times 2.0$ mm^3), quality (no statement as to excitatory or inhibitory process is possible), directionality (inability to distinguish between afferent and efferent pathways), and the accuracy to separate crossing from bending fibers close to midline. To minimize the latter problem we performed additional DTI analyses focusing on crossing brainstem fibers. However, the methods are limited with respect to the identification of pathways crossing twice from the ipsilateral to the contralateral and back to the ipsilateral side. Finally, we lack a statement concerning the strength of the pathways. Another methodical limitation might be seen in the reported presence of magnetic vestibular stimulation (MVS) by static magnetic fields (Roberts et al. 2011, Mian et al. 2013). This is especially important in functional paradigm studies, since conclusions are warranted in comparison with so-called control conditions. However, firstly the resting-state analyses do not require such a comparison with a control condition and secondly the effect of MVS should be a constant activation level that is subtracted by filtering, the removal of the mean signal over time and voxel-wise variability normalization. The last methodical limitation lies within our ROIs. It is important to note that our analyses only apply to one specific PIVC node.

Conclusion

The most important findings regarding the main questions of the study were as follows:

(i) There is congruence in the functional and structural vestibular connectivities between the vestibular nuclei and the ipsilateral and contralateral core regions of the PIVC.
(ii) Crossing and non-crossing vestibular brainstem fibers provide a rope ladder system for the central vestibular network between the vestibular nuclei and the core region of the PIVC.
(iii) Vestibular pathways project through both the posterolateral and the paramedian thalamus.
(iv) A part of the ipsilateral projections directly reach the inferior part of the insula, thus bypassing the thalamic relay station.

(v) The vestibular core regions are interhemispherically connected through the antero-caudal splenium of the corpus callosum.

(vi) Although the dominance of the cortical representation was not a particular question, the data support the earlier described vestibular dominance of the right (non-dominant) hemisphere in right-handers.

Acknowledgments The study was partially funded by the Support Programme for Research and Teaching (Foerderprogramm fuer Forschung und Lehre, FöFoLe^{LMU}), Graduate School of Systemic Neurosciences (GSN), the German Foundation for Neurology (Deutsche Stiftung für Neurologie, DSN), the Hertie Foundation, and the German Federal Ministry of Education and Research (German Center for Vertigo and Balance Disorders-IFB^{LMU} under the Grant code EO 0901). This is a part of the dissertation of T. Hergenroeder. We thank J. Benson for copyediting the manuscript.

Conflict of interest The authors declare that they have no competing financial interests.

References

Akbarian S, Grüsser OJ, Guldin WO (1993) Corticofugal projections to the vestibular nuclei in squirrel monkeys: further evidence of multiple cortical vestibular fields. J Comp Neurol 332:89–104

Akert K, Hartmann-von Monakow K (1980) Relationships of precentral premptor and prefrontal cortex to the mediodorsal and intralaminar nuclei of the monkey thalamus. Acta Neurobiol Exp (Warsz.) 40:7–20

Alexander GE, Crutcher MD, DeLong MR (1990) Basal ganglia–thalamocortical circuits: parallel substrates for motor, oculomotor, "prefrontal" and "limbic" functions. Prog Brain Res 85:119–146

Asanuma C, Thach WT, Jones EG (1983) Distribution of cerebellar terminations and their relation to other afferent terminations in the ventral lateral thalamic region of the monkey. Brain Res 286:237–265

Ashburner J (2007) A fast diffeomorphic image registration algorithm. Neuroimage 38:95–113

Baier B, Thömke F, Wilting J, Heinze C, Geber C, Dieterich M (2012) A pathway in the brainstem for roll-tilt of the subjective visual vertical: evidence from a lesion-behavior mapping study. J Neurosci 32:14854–14858

Baumgartner U, Iannetti GD, Zambreanu L, Stoeter P, Treede RD, Tracey I (2010) Multiple somatotopic representations of heat and mechanical pain in the operculo-insular cortex: a high-resolution fMRI study. J Neurophysiol 104:2863–2872

Becker HGT, Haarmeier T, Tatagiba M, Gharabaghi A (2013) Electrical stimulation of the human homolog of the medial superior temporal area induces visual motion blindness. J Neurosci 33:18288–18297

Behrens TE, Sporns O (2012) Human connectomics. Curr Opin Neurobiol 22:144–153

Behrens TE, Johansen-Berg H, Woolrich MW, Smith SM, Wheeler-Kingshott CA, Boulby PA, Barker GJ, Sillery EL, Sheehan K, Ciccarelli O, Thompson AJ, Brady JM, Matthews PM (2003a) Non-invasive mapping of connections between human thalamus and cortex using diffusion imaging. Nat Neurosci 6:750–757

Behrens TE, Woolrich MW, Jenkinson M, Johansen-Berg H, Nunes RG, Clare S, Matthews PM, Brady JM, Smith SM (2003b) Characterization and propagation of uncertainty in diffusion-weighted MR imaging. Magn Reson Med 50:1077–1088

Behrens TE, Berg HJ, Jbabdi S, Rushworth MF, Woolrich MW (2007) Probabilistic diffusion tractography with multiple fibre orientations: what can we gain? NeuroImage 34:144–155

Behzadi Y, Restom K, Liau J, Liu TT (2007) A component based noise correction method (CompCor) for BOLD and perfusion based fMRI. NeuroImage 37:90–101

Benjamini Y, Hochberg Y (1995) Controlling the false discovery rate: a practical and powerful approach to multiple testing. J R Stat Soc, Ser B (Methodological) 57(1):289–300

Bense S, Stephan T, Yousry TA, Brandt T, Dieterich M (2001) Multisensory cortical signal increases and decreases during vestibular galvanic stimulation (fMRI). J Neurophysiol 85:886–899

Berthoz A, Grantyn A (1986) Neuronal mechanisms underlying eye–head coordination. In: Freund HJ, Büttner U, Cohen B, Noth J (eds) The oculomotor and skeletal motor systems: progress in brain research, vol 64. Elsevier, Amsterdam, pp 325–343

Bingel U, Glascher J, Weiller C, Buchel C (2004) Somatotopic representation of nociceptive information in the putamen: an event-related fMRI study. Cereb Cortex 14:1340–1345

Blum PS, Day MJ, Carpenter MB, Gilman S (1979a) Thalamic components of the ascending vestibular system. Exp Neurol 64:587–603

Blum PS, Abraham LD, Gilman S (1979b) Vestibular, auditory, and somatic input to the posterior thalamus of the cat. Exp Brain Res 34:1–9

Brandt T, Dieterich M (1994) Vestibular syndromes in the roll plane: topographic diagnosis from brainstem to cortex. Ann Neurol 36:337–347

Brandt T, Dieterich M (1998) Two types of ocular tilt reaction: the 'ascending' pontomedullary VOR-OTR and the 'descending' mesencepahlic integrator-OTR. Neuro-ophthalmology 19:83–92

Brandt T, Dieterich M (1999) The vestibular cortex. Its locations, functions, and disorders. Ann N Y Acad Sci 871:293–312

Brandt T, Bucher SF, Seelos KC, Dieterich M (1998) Bilateral functional MRI activation of the basal ganglia and middle temporal/medial superior temporal motion-sensitive areas: optokinetic stimulation in homonymous hemianopia. Arch Neurol 55:1126–1131

Bucher SF, Dieterich M, Wiesmann M, Weiss A, Zink R, Yousry TA, Brandt T (1998) Cerebral functional magnetic resonance imaging of vestibular, auditory, and nociceptive areas during galvanic stimulation. Ann Neurol 44:120–125

Büttner U, Henn V (1976) Thalamic unit activity in the alert monkey during natural vestibular stimulation. Brain Res 103:127–132

Büttner-Ennever JA (1992) Patterns of connectivity in the vestibular nuclei. Ann N Y Acad Sci 656:363–378

Büttner-Ennever JA (1999) A review of otolith pathways to brainstem and cerebellum. Ann N Y Acad Sci 871:51–64

Büttner-Ennever JA, Horn AKE (2014) Olszewski and Baxter's cytoarchitecture of the human brainstem. S Karger AG, Basel 3rd revised and extended edition

Ceballos-Baumann AO, Boecker H, Fogel W, Alesch F, Bartenstein P, Conrad B, Diederich N, von Falkenhayn I, Moringlane JR, Schwaiger M, Tronnier VM (2001) Thalamic stimulation for essential tremor activates motor and deactivates vestibular cortex. Neurology 56:1347–1354

Chen A, DeAngelis GC, Angelaki DE (2010) Macaque parieto-insular vestibular cortex: responses to self-motion and optic flow. J Neurosci 30:3022–3042

Chen A, DeAngelis GC, Angelaki DE (2011a) Convergence of vestibular and visual self-motion signals in an area of the posterior sylvian fissure. J Neurosci 31:11617–11627

Chen A, DeAngelis GC, Angelaki DE (2011b) A comparison of vestibular spatiotemporal tuning in macaque parietoinsular vestibular cortex, ventral intraparietal area, and medial superior temporal area. J Neurosci 31:3082–3094

Conrad J, Baier B, Dieterich M (2014) The role of the thalamus in the human subcortical vestibular system. J Vestib Res. doi:10.3233/VES-140534

Cumbley J, Worseley K, Flandin G, Friston K (2010) Topological FDR for neuroimaging. Neuroimage 49:3057–3064

Dauguet J, Peled S, Berezovskii V, Delzescaux T, Warfield SK, Born R, Westin CF (2007) Comparison of fiber tracts derived from in vivo DTI tractography with 3D histological neural tract tracer reconstruction on a macaque brain. NeuroImage 37:530–538

Deecke L, Schwarz DW, Fredrickson JM (1973) Response patterns of vestibular thalamic neurons in the rhesus monkey. Int J Equilib Res 3:4–7

Desikan RS, Segonne F, Fischl B, Quinn BT, Dickerson BC, Blacker D, Buckner RL, Dale AM, Maguire RP, Hyman BT, Albert MS, Killiany RJ (2006) An automated labeling system for subdividing the human cerebral cortex on MRI scans into gyral based regions of interest. NeuroImage 31:968–980

Dieringer H (1995) 'Vestiblar compensation': neural plasticity and its relations to functional recovery after labyrinthine lesions in frogs and other vertebrates. Prog Neurobiol 46:97–129

Dieterich M (2007) Functional brain imaging: a window into the visuo-vestibular systems. Curr Opin Neurol 20:12–18

Dieterich M, Brandt T (1993a) Ocular torsion and tilt of subjective visual vertical are sensitive brainstem signs. Ann Neurol 33:292–299

Dieterich M, Brandt T (1993b) Thalamic infarctions: differential effects on vestibular function in the roll plane (35 patients). Neurology 43:1732–1740

Dieterich M, Brandt T (2008) Functional brain imaging of peripheral and central vestibular disorders. Brain 131:2538–2552

Dieterich M, Bucher SF, Seelos KC, Brandt T (1998) Horizontal or vertical optokinetic stimulation activates visual motion-sensitive, ocular motor and vestibular cortex areas with right hemispheric dominance. An fMRI study. Brain 121:1478–1495

Dieterich M, Bense S, Lutz S, Drzezga A, Stephan T, Bartenstein P, Brandt T (2003) Dominance for vestibular cortical function in the non-dominant hemisphere. Cereb Cortex 13:994–1007

Dieterich M, Bartenstein P, Spiegel S, Bense S, Schwaiger M, Brandt T (2005) Thalamic infarctions cause side-specific suppression of vestibular cortex activations. Brain 128:2052–2067

Eggers SDZ, Zee DS (2010) Handbook of clinical neurophysiology. Vertigo and imbalance: clinical neurophysiology of the vestibular system, vol 9. Elsevier, Amsterdam

Eickhoff SB, Stephan KE, Mohlberg H, Grefkes C, Fink GR, Amunts K, Zilles K (2005) A new SPM toolbox for combining probabilistic cytoarchitectonic maps and functional imaging data. NeuroImage 25:1325–1335

Eickhoff SB, Heim S, Zilles K, Amunts K (2006a) Testing anatomically specified hypotheses in functional imaging using cytoarchitectonic maps. NeuroImage 32:570–582

Eickhoff SB, Weiss PH, Amunts K, Fink GR, Zilles K (2006b) Identifying human parieto-insular vestibular cortex using fMRI and cytoarchitectonic mapping. Hum Brain Mapp 27:611–621

Elwischger K, Rommer P, Prayer D, Mueller C, Auff E, Wiest G (2012) Thalamic astasia from isolated centromedian thalamic infarction. Neurology 78:146–147

Emri M, Kisely M, Lengyel Z, Balkay L, Marian T, Miko L, Berenyi E, Sziklai I, Tron L, Toth A (2003) Cortical projection of peripheral vestibular signaling. J Neurophysiol 89:2639–2646

Fasold O, von Brevern M, Kuhberg M, Ploner CJ, Villringer A, Lempert T, Wenzel R (2002) Human vestibular cortex as identified with caloric stimulation in functional magnetic resonance imaging. NeuroImage 17:1384–1393

Fox MD, Raichle ME (2007) Spontaneous fluctuations in brain activity observed with functional magnetic resonance imaging. Nat Rev Neurosci 8:700–711

Fox MD, Snyder AZ, Vincent JL, Corbetta M, Van Essen DC, Raichle ME (2005) The human brain is intrinsically organized into dynamic, anticorrelated functional networks. Proc Natl Acad Sci U S A 102:9673–9678

Fukushima K, Fukushima J, Terashima T (1987) The pathways responsible for the characteristic head posture produced by lesions of the interstitial nucleus of Cajal in the cat. Exp Brain Res 68:88–102

Goldberg JM, Wilson VJ, Cullen KE, Angelaki DE, Broussard DM, Büttner-Ennever JA, Fukushima K, Minor LB (2012) The vestibular system. A sixth sense. Oxford University Press, New York

Graf W, Ezure K (1986) Morphology of vertical canal related second order vestibular neurons in the cat. Exp Brain Res 63:35–48

Green AM, Angelaki DE (2004) An integrative neural network for detecting inertial motion and head orientation. J Neurophysiol 92:905–925

Greicius MD, Supekar K, Menon V, Dougherty RF (2009) Resting-state functional connectivity reflects structural connectivity in the default mode network. Cereb Cortex 19:72–78

Grüsser OJ, Pause M, Schreiter U (1990a) Localization and responses of neurones in the parieto-insular vestibular cortex of awake monkeys (Macaca fascicularis). J Physiol 430:537–557

Grüsser OJ, Pause M, Schreiter U (1990b) Vestibular neurones in the parieto-insular cortex of monkeys (Macaca fascicularis): visual and neck receptor responses. J Physiol 430:559–583

Guldin WO, Grüsser OJ (1998) Is there a vestibular cortex? Trends Neurosci 21:254–259

Guldin WO, Akbarian S, Grüsser OJ (1992) Cortico-cortical connections and cytoarchitectonics of the primate vestibular cortex: a study in squirrel monkeys (Saimiri sciureus). J Comp Neurol 326:375–401

Halmagyi GM, Curthoys IS (1988) A clinical sign of canal paresis. Arch Neurol 45:737–739

Hammers A, Allom R, Koepp MJ, Free SL, Myers R, Lemieux L, Mitchell TN, Brooks DJ, Duncan JS (2003) Three-dimensional maximum probability atlas of the human brain, with particular reference to the temporal lobe. Hum Brain Mapp 19:224–247

Hassler R (1959) Anatomy of the thalamus. In: Schaltenbrand G, Bailey P (eds) Introduction to stereotaxis with an atlas of the human brain, vol 1. Thieme, Stuttgart, pp 230–290

Hawrylyshyn PA, Rubin AM, Tasker RR, Organ LW, Fredrickson M (1978) Vestibulothalamic projections in man—a sixth primary sensory pathway. J Neurophysiol 41:394–401

Hofer S, Frahm J (2006) Topography of the human corpus callosum revisited- comprehensive fiber tractography using diffusion tensor magnetic resonance imaging. Neuroimage 32:989–994

Hyam JA, Owen SL, Kringelbach ML, Jenkinson N, Stein JF, Green AL, Aziz TZ (2012) Contrasting connectivity of the ventralis intermedius and ventralis oralis posterior nuclei of the motor thalamus demonstrated by probabilistic tractography. Neurosurgery 70:162–169

Janzen J, Schlindwein P, Bense S, Bauermann T, Vucurevic G, Stoeter P, Dieterich M (2008) Neural correlates of hemispheric dominance and ipsilaterality within the vestibular system. Neuroimage 42(4):1508–1518

Jenkinson M, Bannister P, Brady M, Smith S (2002) Improved optimization for the robust and accurate linear registration and motion correction of brain images. NeuroImage 17:825–841

Jenkinson M, Beckmann CF, Behrens TE, Woolrich MW, Smith SM (2012) Fsl. NeuroImage 62:782–790

Johansen-Berg H, Rushworth MF (2009) Using diffusion imaging to study human connectional anatomy. Annu Rev Neurosci 32:75–94

Kayahara T, Yasui Y, Nakano K (1994) Pallidal afferents to the neurons in the anterior thalamic reticular nucleus projecting to the centromedian nucleus. In: Percheron G, McKenzie JS, Feger J (eds) The basal ganglia, vol IV. Plenum Press, New York, pp 121–125

Kim R, Nakano K, Jayaraman A, Carpenter MB (1976) Projection of the globus pallidus and adjacent structures: an autoradiographic study in the monkey. J Comp Neurol 169:263–289

Konen CS, Kastner S (2008) Representation of eye movements and stimulus motion in topographically organized areas of human posterior parietal cortex. J Neurosci 28:8361–8375

Lang W, Buttner-Ennever JA, Buttner U (1979) Vestibular projections to the monkey thalamus: an autoradiographic study. Brain Res 177:3–17

Lee PH, Lee JH, Joo US (2005) Thalamic infarct presenting with thalamic astasia. Eur J Neurol 12:317–319

Lopez C, Blanke O (2011) The thalamocortical vestibular system in animals and humans. Brain Res Rev 67:119–146

Maciewicz R, Phipps BS, Bry J, Highstein SM (1982) The vestibulothalamic pathway: contribution of the ascending tract of Deiters. Brain Res 252:1–11

Makris N, Goldstein JM, Kennedy D, Hodge SM, Caviness VS, Faraone SV, Tsuang MT, Seidman LJ (2006) Decreased volume of left and total anterior insular lobule in schizophrenia. Schizophr Res 83:155–171

Masdeu JC, Gorelick PB (1988) Thalamic astasia: inability to stand after unilateral thalamic lesions. Ann Neurol 23:596–603

Maunsell JH, Newsome WT (1987) Visual processing in monkey extrastriate cortex. Annu Rev Neurosci 10:363–401

McGuinness CM, Krauthammer GM (1980) The afferent projections to the centrum medianum of the cat as demonstrated by retrograde transport of horseradish peroxidase. Brain Res 184:255–269

Mian OS, Li Y, Antunes A, Glover PM, Day BL (2013) On vertigo due to static magnetic fields. PLoS One 8:e78748

Miller WL, Maffei V, Bosco G, Iosa M, Zago M, Macaluso E, Lacquaniti F (2008) Vestibular nuclei and cerebellum put visual gravitational motion in context. J Neurophysiol 99:1969–1982

Morel A (2007) Stereotactic Atlas of the Human Thalamus and Basal Ganglia. Informa Heathcare USA Inc, New York

Oldfield RC (1971) The assessment and analysis of handedness: the Edinburgh inventory. Neuropsychologia 9:97–113

Poldrack RA, Fletcher PC, Henson RN, Worsley KJ, Brett M, Nichols TE (2008) Guidelines for reporting an fMRI study. NeuroImage 40:409–414

Power JD, Barnes KA, Snyder AZ, Schlaggar BL, Petersen SE (2012) Spurious but systematic correlations in functional connectivity MRI networks arise from subject motion. NeuroImage 59:2142–2154

Putnam MC, Steven MS, Doron KW, Riggall AC, Gazzaniga MS (2010) Cortical projection topography of the human splenium: hemispheric asymmetry and individual differences. J Cogn Neurosci 22:1662–1669

Roberts DC, Marcelli V, Gillen JS, Carey JP, Della Santina CC, Zee DS (2011) MRI magnetic field stimulates rotational sensors of the brain. Curr Biol 21:1635–1640

Robinson FR, Phillips JO, Fuchs AF (1994) Coordinations of gaze shifts in primates: brainstem inputs to neck and extraocular motoneuron pools. J Comp Neurol 346:43–62

Salmaso D, Longoni AM (1985) Problems in the assessment of hand preference. Cortex 21:533–549

Sans A, Raymond J, Marty R (1970) Thalamic and cortical responses to electric stimulation of the vestibular nerve in the cat. Exp Brain Res 10:265–275

Schlag J, Schlag-Ray M (1984) Visuomotor functions of central thalamus in monkey. II. Unit activity related to visual events, targeting, and fixation. J Neurophysiol 51:1175–1195

Schneider E, Villgrattner T, Vockeroth J, Bartl K, Kohlbecher S, Bardins S, Ulbrich H, Brandt T (2009) EyeSeeCam: an eye movement-driven head camera for the examination of natural visual exploration. Ann N Y Acad Sci 1164:461–467

Shiroyama T, Kayahara T, Yasui Y, Nomura J, Nakano K (1999) Projections of the vestibular nuclei to the thalamus in the rat: a phaseolus vulgaris leucoagglutinin study. J Comp Neurol 407:318–332

Smith SM (2002) Fast robust automated brain extraction. Hum Brain Mapp 17:143–155

Smith SM, Jenkinson M, Woolrich MW, Beckmann CF, Behrens TE, Johansen-Berg H, Bannister PR, De Luca M, Drobnjak I, Flitney DE, Niazy RK, Saunders J, Vickers J, Zhang Y, De Stefano N, Brady JM, Matthews PM (2004) Advances in functional and structural MR image analysis and implementation as FSL. NeuroImage 23(Suppl 1):S208–S219

Straka H, Dieringer N (2004) Basic organization principles of the VOR: lessons from frogs. Prog Neurobiol 73:259–309

Tasker RR, Organ LW, Hawrylyshyn P (1982) Investigation of the surgical target for alleviation of involuntary movement disorders. Applied Neurophysiology 45:261–274

Uchino Y, Hirai N, Suzuki S, Watanabe S (1981) Properties of secondary vestibular neurons fired by stimulation of ampullary nerve of the vertical, anterior or posterior, semicircular canals in the cat. Brain Res 223:273–286

van den Heuvel MP, Mandl RC, Kahn RS, Hulshoff Pol HE (2009) Functionally linked resting-state networks reflect the underlying structural connectivity architecture of the human brain. Hum Brain Mapp 30:3127–3141

Van Dijk KR, Sabuncu MR, Buckner RL (2012) The influence of head motion on intrinsic functional connectivity MRI. NeuroImage 59:431–438

Westheimer G, Blair SM (1975) The ocular tilt reaction—a brainstem oculomotor routine. Investigative Ophthalmology 14:833–839

Whitfield-Gabrieli S, Nieto-Castanon A (2012) Conn: a functional connectivity toolbox for correlated and anticorrelated brain networks. Brain Connectivity 2:125–141

Witelson SF (1989) Hand and sex differences in the isthmus and genu of the human coprus callosum. A postmortem morphological study. Brain 112:799–835

Woolrich MW, Jbabdi S, Patenaude B, Chappell M, Makni S, Behrens T, Beckmann C, Jenkinson M, Smith SM (2009) Bayesian analysis of neuroimaging data in FSL. NeuroImage 45:S173–S186

Zhang D, Snyder AZ, Shimony JS, Fox MD, Raichle ME (2010) Noninvasive functional and structural connectivity mapping of the human thalamocortical system. Cereb Cortex 20:1187–1194

zu Eulenburg P, Caspers S, Roski C, Eickhoff SB (2012) Meta-analytical definition and functional connectivity of the human vestibular cortex. NeuroImage 60:162–169

Zwergal A, Büttner-Ennever J, Brandt T, Strupp M (2008) An ipsilateral vestibulothalamic tract adjacent to the medial lemniscus in humans. Brain 131:2928–2935

Zwergal A, Strupp M, Brandt T, Büttner-Ennever JA (2009) Parallel ascending vestibular pathways: anatomical localization and functional specialization. Ann N Y Acad Sci 1164:51–59